

Conditional Consistency Guided Image Translation and Enhancement

A. V. Subramanyam, Amil Bhagat, Milind Jain

Indraprastha Institute of Information Technology (IIIT), Delhi, India

Email: {subramanyam@iiitd.ac.in, amil21309@iiitd.ac.in, milind21165@iiitd.ac.in}

Abstract—Consistency models have emerged as a promising alternative to diffusion models, offering high-quality generative capabilities through single-step sample generation. However, their application to multi-domain image translation tasks, such as cross-modal translation and low-light image enhancement remains largely unexplored. In this paper, we introduce Conditional Consistency Models (CCMs) for multi-domain image translation by incorporating additional conditional inputs. We implement these modifications by introducing task-specific conditional inputs that guide the denoising process, ensuring that the generated outputs retain structural and contextual information from the corresponding input domain. We evaluate CCMs on 10 different datasets demonstrating their effectiveness in producing high-quality translated images across multiple domains. Code is available <https://github.com/amilbhagat/Conditional-Consistency-Models>.

Index Terms—Conditional synthesis, consistency models, cross-modal translation, low-light image enhancement, medical image translation

I. INTRODUCTION

Generative modelling has witnessed rapid progress in recent years, evolving from the early successes of Generative Adversarial Networks (GANs) [1] to the more stable and controllable diffusion models [2]. In the early stages, the introduction of conditional GANs (cGANs) [3] made it possible to guide the generation process using auxiliary information such as class labels or paired images. This allowed models to learn structured mappings between input and target domains in a variety of conditional image-to-image translation tasks, including semantic segmentation, image synthesis, style transfer and other applications [4], [5]. Despite their successes, conditional GANs often suffer from mode collapse, training instability, and the necessity of intricate adversarial training schemes.

On the other hand, score-based diffusion models [2] have emerged as a robust alternative for image generation and translation. These models add noise to the data and learn to invert this process via score estimation, producing high-quality outputs. However, these models require many iterative steps to produce high quality images. Recently, consistency models [6] have been proposed as a new class of generative models. Instead of relying on iterative refinement steps like diffusion, consistency models directly learn mappings from any noise level to data.

However, despite their advantages, consistency models have been explored primarily in unconditional settings. The extension of these models to conditional, multi-domain tasks

remains under-explored. This paper focuses on two representative tasks of significant practical value and complexity: cross-modal translation and low-light image enhancement (LLIE).

Cross-modal translation is a crucial task in surveillance and medical systems where different modalities may reveal complementary information. The LLVIP dataset [7] exemplifies the significance of this translation, as methods must effectively learn visible to infrared mappings while preserving the spatial details. Similarly, BCI [8] provides a challenging medical dataset of paired hematoxylin and eosin (HE) and immunohistochemical techniques (IHC) images. As routine diagnosis with IHC is very expensive, translation task from HE to IHC can be very helpful in bringing down the overall cost. On the other hand, LLIE is critical in computer vision applications where images suffer from insufficient illumination, leading to poor image details. Methods such as SID [9], GSAD [10] have demonstrated impressive results using data-driven approaches trained on paired dark and well-exposed images. Nonetheless, these methods often rely on adversarial training setups which are known to have convergence issues, or explicit iterative sampling strategy which is time consuming.

While existing approaches to these problems range from traditional Retinex-based methods [11] to deep convolutional neural networks [9], many either lack the adaptability required for multi-domain translation or are computationally expensive at inference time. Conditional diffusion models can produce excellent results but at the cost of significant computational overhead during sampling [12]. Conditional GANs, though fast, may exhibit mode collapse or require carefully tuned adversarial training setups [13].

In this work, we introduce Conditional Consistency Models (CCMs) for multi-domain image translation tasks. CCMs innovate on traditional consistency models by incorporating additional conditional inputs, such as, visible image for visible to infrared translation, HE image for HE to IHC translation, and low-light image for LLIE, respectively. By carefully designing the network architecture to take the conditional input and training process, CCMs yield highly efficient inference while preserving important local and global spatial details from the conditional input. Unlike other techniques, our method is applicable for both translation and image enhancement.

II. RELATED WORKS

A. Cross-modal Image Translation

Generative approaches for image translation have evolved significantly. In case of visible to infrared translation, GAN-based methods have been widely explored, and models such as ThermalGAN [14], TMGAN [15], and InfraGAN [16] have achieved notable success in generating high-quality IR images. These methods often require paired RGB-IR datasets, which are scarce in practice. Lee *et al.* propose an unsupervised method using edge-guidance and style control in a multi-domain image translation framework. MappingFormer [17] uses low and high frequency features for visible to infrared image generation. These features are fused and a dual contrast learning module further finds an effective mapping between the unpaired data. Similarly, [18] also study the unpaired data translation.

In case of medical images, BCI [8] addresses translation of HE images to IHC images. They propose a multi-scale structure in a Pix2Pix framework. The multi-scale pyramid enables the model to capture both global and local features effectively leading to improved image generation quality. On similar lines, GAN based translation is investigated in [19]–[21].

B. Low Light Image Enhancement

GAN Based Methods: EnlightenGAN [22] adopts a global and local discriminator to directly map low-light images to normal-light images. This is trained in unsupervised manner. Similarly, other unsupervised methods show further improvement in the enhanced images [23].

Diffusion Based Methods: Diff-Retinex [24] combines Retinex decomposition with diffusion-based conditional generation. It separates images into illumination and reflectance components, which are then adjusted using diffusion networks. ExposureDiffusion [25] integrates physics-based exposure processes with a diffusion model. Instead of starting from pure noise, it begins with noisy images. It uses adaptive residual layers to refine image details and achieves better generalization and performance with fewer parameters. AnlightenDiff [26] formulates the problem of LLIE as residual learning. It decomposes the difference between normal and low light image into a residual component and a noise term. PyDiff [27] introduces a pyramid resolution sampling strategy to speed up the diffusion process and employs a global corrector to address degradation issues. GSAD [10] uses a curvature-regularized trajectory in the diffusion process to preserve fine details and enhance global contrast. It also incorporates uncertainty-guided regularization to adaptively focus on challenging regions. These methods use paired datasets.

C. Preliminaries: Consistency Models

Consider a continuous trajectory $\{\mathbf{r}_t\}_{t \in [\epsilon, T]}$ connecting a clean data sample \mathbf{r}_ϵ at time ϵ to a noisy sample \mathbf{r}_T at a larger time T . The probability flow ODE ensures a bijective mapping between data and noise at different time scales. A consistency model [6] leverages this structure to learn a direct,

single-step mapping from a noisy sample at any time t back to the clean sample \mathbf{r}_ϵ . Formally, a consistency model defines a consistency function g_ϕ such that:

$$g_\phi(\mathbf{r}_t, t) = \mathbf{r}_\epsilon \quad \forall t \in [\epsilon, T]. \quad (1)$$

This *self-consistency* property ensures that no matter the noise level t , the model consistently recovers the same underlying clean data sample.

Boundary Condition and Parameterization: A key requirement is the *boundary condition*, stating that at the minimal noise level ϵ , the model should act as the identity $g_\phi(\mathbf{r}_\epsilon, \epsilon) = \mathbf{r}_\epsilon$. To naturally incorporate this condition, consistency models employ a parameterization that respects this constraint. A common approach uses a combination of skip connections and time-dependent scaling:

$$g_\phi(\mathbf{r}, t) = a_{\text{skip}}(t) \mathbf{r} + a_{\text{out}}(t) G_\phi(\mathbf{r}, t), \quad (2)$$

where, $a_{\text{skip}}(t)$ and $a_{\text{out}}(t)$ are scalar functions of t that regulate the contributions of the input \mathbf{r} and the learned function $G_\phi(\mathbf{r}, t)$, respectively. The boundary condition is satisfied by setting $a_{\text{skip}}(\epsilon) = 1$ and $a_{\text{out}}(\epsilon) = 0$, ensuring that $g_\phi(\mathbf{r}, \epsilon) = \mathbf{r}$.

As the noise scale t increases, the influence of $G_\phi(\mathbf{r}, t)$ grows through $a_{\text{out}}(t)$, allowing the model to move away from the identity mapping and perform increasingly complex denoising transformations. This parameterization naturally embeds the boundary condition in the model structure and maintains differentiability across noise scales.

Training Consistency Models: Training a consistency model involves enforcing self-consistency at multiple noise levels. Given a sample \mathbf{r} , a noise vector $\mathbf{z} \sim \mathcal{N}(\mathbf{0}, \mathbf{I})$, and a pair of noise scales $(t_n, t_{n+1}) \in [\epsilon, T]$, we form noisy inputs $\mathbf{r}_{t_n} = \mathbf{r} + t_n \mathbf{z}$, $\mathbf{r}_{t_{n+1}} = \mathbf{r} + t_{n+1} \mathbf{z}$. The model g_ϕ should produce the same clean output \mathbf{r}_ϵ for both \mathbf{r}_{t_n} and $\mathbf{r}_{t_{n+1}}$. Thus, the training loss encourages:

$$g_\phi(\mathbf{r}_{t_{n+1}}, t_{n+1}) = g_\phi(\mathbf{r}_{t_n}, t_n) = \mathbf{r}_\epsilon.$$

By minimizing a suitable distance measure between these outputs, the network learns to invert the noise injection step at any arbitrary noise level t .

III. PROPOSED METHOD

Given a paired dataset $\mathcal{D} = \{\mathbf{v}_i, \mathbf{r}_i\}_{i=1}^N$ of RGB $\mathbf{v}_i \in \mathbb{R}^{H \times W \times C}$ and its corresponding pair $\mathbf{r}_i \in \mathbb{R}^{H \times W \times C}$. In case of visible to infrared image translation, \mathbf{v} is the RGB image and \mathbf{r} is the infrared image. For BCI dataset [8], \mathbf{v} is the HE image and \mathbf{r} is the IHC image. In case of LLIE, \mathbf{v} is the ill-exposed image and \mathbf{r} is the well-exposed image. Our aim is to learn a mapping from a given input and condition image to its respective paired image. More formally, we learn a function $G : \mathbf{v} \times \mathbf{r} \rightarrow \mathbf{r}$, where $\mathbf{v} \times \mathbf{r}$ denotes a pair. In our proposed method, G is parameterized via a consistency model [28]. In order to generate images which semantically align with the input image, we make use of conditional synthesis. Here, we use an image pair (\mathbf{v}, \mathbf{r}) as the condition and input, respectively, and train the model to generate only \mathbf{r} . Figure 1 illustrates the proposed method.

A. Conditional Consistency

To adapt consistency models to conditional multi-domain image translation, we introduce a conditional input \mathbf{v} . We define the conditional consistency function as,

$$g_\phi(\mathbf{r}, \mathbf{v}, t) = \begin{cases} \mathbf{r} & t = \epsilon, \\ G_\phi(\mathbf{r}, \mathbf{v}, t), & t \in (\epsilon, T], \end{cases} \quad (3)$$

where \mathbf{v} provides conditional information that guides the denoising process. As g_ϕ inverts the noise injection step, it also conditions on \mathbf{v} to ensure that the generated image \mathbf{r} corresponds to the infra-red, IHC, or well-exposed pair of \mathbf{v} .

In addition, the consistency function must follow the boundary condition, that is:

$$g_\phi(\mathbf{r}_\epsilon, \mathbf{v}, \epsilon) = \mathbf{r}_\epsilon. \quad (4)$$

As the consistency function must map noisy data from any time-step to the clean data, using eq 3 and eq 4, we can write,

$$g_\phi(\mathbf{r}_{t_{n+1}}, \mathbf{v}, t_{n+1}) = g_\phi(\mathbf{r}_{t_n}, \mathbf{v}, t_n) = \mathbf{r}_\epsilon.$$

We parameterize the conditional consistency model as,

$$g_\phi(\mathbf{r}, \mathbf{v}, t) = a_{\text{skip}}(t)\mathbf{r} + a_{\text{out}}(t)G_\phi(\mathbf{r}, \mathbf{v}, t). \quad (5)$$

In eq 5, the boundary condition, where $g_\phi(\mathbf{r}, \mathbf{v}, t) = \mathbf{r}$, is obtained for $t = \epsilon$, $a_{\text{skip}}(\epsilon) = 1$ and $a_{\text{out}}(\epsilon) = 0$. This ensures that the model outputs the clean image \mathbf{r} at the minimal noise scale. As the noise scale increases, the generative component $G_\phi(\mathbf{r}, \mathbf{v}, t)$ plays a more significant role, allowing the network to learn complex transformations required for translating \mathbf{v} into \mathbf{r} . We present the training process in Algorithm 1.

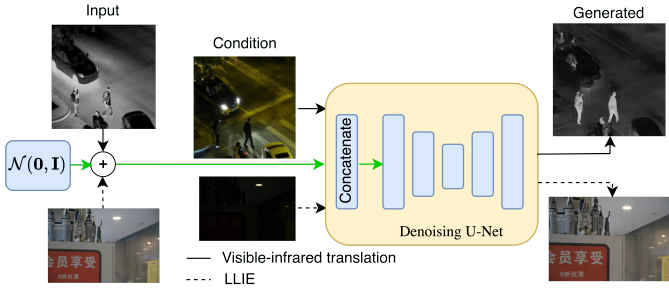


Fig. 1. Model Architecture. Our model can take a pair of visible-infrared, HE-IHC, or, low light and well-exposed images. Visible, HE or low light image acts as a conditional input. The noise as per time step t is added to the input infrared, IHC or well exposed image. This noisy image is then concatenated with the condition input and fed to the U-Net. The model can be sampled to obtain the infrared, IHC or enhanced image.

B. Training and Sampling

Training Algorithm: In order to generate the desired output given the inputs, we make use of conditional synthesis. Here, we use an image pair (\mathbf{v}, \mathbf{r}) as the input and train the model to generate only \mathbf{r} . G_ϕ takes a $2C$ channel input and gives a C channel output. In our method, we concatenate \mathbf{v} and \mathbf{r} across channels to obtain a $2C$ channel input. \mathbf{v} only acts as a conditional input and we do not add any noise to it.

We adopt the step schedule $M(\cdot)$ as given in [28] and the distance function $d(\cdot, \cdot)$ is pseudo-Huber loss given in [28].

Algorithm 1: Conditional Consistency Training (CCT)

Input: Paired dataset $\mathcal{D} = \{(\mathbf{v}_i, \mathbf{r}_i)\}_{i=1}^N$, initial model parameter ϕ , learning rate η , step schedule $M(\cdot)$, distance function $d(\cdot, \cdot)$, weighting function $\lambda(\cdot)$

Initialize $\phi^- \leftarrow \phi$, $k \leftarrow 0$;

repeat

Sample $(\mathbf{v}, \mathbf{r}) \sim \mathcal{D}$ and $n \sim U[1, M(k) - 1]$

Sample $\mathbf{z} \sim \mathcal{N}(\mathbf{0}, \mathbf{I})$

Compute the loss:

$$\mathcal{L}(\phi, \phi^-) \leftarrow \lambda(t_n) d(g_\phi(\mathbf{r} + t_{n+1}\mathbf{z}, \mathbf{v}, t_{n+1}), g_{\phi^-}(\mathbf{r} + t_n\mathbf{z}, \mathbf{v}, t_n))$$

Update the model parameters:

$$\phi \leftarrow \phi - \eta \nabla_\phi \mathcal{L}(\phi, \phi^-)$$

$$\phi^- \leftarrow \phi$$

Increment $k \leftarrow k + 1$

until Convergence;

Sampling : The unconditional sampling procedure starts from Gaussian noise $\hat{\mathbf{r}}_T$ and evaluates the consistency model $\mathbf{r} \leftarrow g_\phi(\hat{\mathbf{r}}_T, T)$. To incorporate conditions, we now have:

$$\mathbf{r} \leftarrow g_\phi(\hat{\mathbf{r}}_T, \mathbf{v}, T). \quad (6)$$

In practice, we concatenate the C channel noise with the condition input \mathbf{v} and evaluate g_ϕ . This modified algorithm ensures that sampling is guided by the conditional input \mathbf{v} . We sample through single-step generation only.

IV. EXPERIMENT

In the experiments we show that our method is applicable to different tasks and based on the conditional input, the paired output can be generated. We compare our results with SOTA methods in image translation and LLIE tasks, and demonstrate that our method achieves competitive results. Additionally, we would like to emphasize that our method generalizes well to medical dataset also.

A. Datasets

We evaluate our proposed method on multiple datasets, including LLVIP [7], BCI [8], LOLv1 [29], LOLv2 [30], and SID [9]. The LLVIP dataset comprises 15,488 pairs of visible and thermal images captured under low-light conditions, of which 12,025 pairs are for training and 3,463 are reserved for testing. The BCI dataset comprises 9,746 images, organized into 4,873 pairs of Hematoxylin and Eosin (HE), and Immunohistochemistry (IHC) images. Among these, 3,896 pairs are used for training, while the remaining 977 pairs are used for testing. LOLv1 comprises 485 training-paired low-light and normal-light images and 15 testing pairs. LOLv2 is divided into LOLv2-real and LOLv2-synthetic subsets, each containing 689 and 900 training pairs and 100 testing pairs,

respectively. For SID dataset, we used the subset captured by the Sony α 7S II camera. It comprises 2,463 short-/long-exposure RAW image pairs, of these, 1,865 image pairs are used for training, while 598 pairs are used for testing. In addition to the above benchmarks, we tested our method on five unpaired datasets, LIME [31], NPE [32], MEF [33] and DICM [34] and VV¹, that are low-light images and used to check the LLIE potential of a model.

B. Implementation Details

LLVIP images are randomly cropped to 512x512 and then resized to 128x128 for training over 1000 epochs. In case of BCI, images are randomly cropped to 256x256 and trained for 500 epochs. LOLv1, LOLv2-real, LOLv2-synthetic and SID images are randomly cropped to 128x128 for training over 500 epochs for SID, and 1500 epochs for the rest. The values of $a_{skip}(t)$, $a_{out}(t)$, $\lambda(t_n)$, $M(\cdot)$, and $d(\cdot, \cdot)$ are set to default values given in [28].

C. Evaluation Metrics

We utilize Peak Signal-to-Noise Ratio (PSNR) and Structural Similarity Index Measure (SSIM) to assess the quality of the generated images. Additionally, for datasets lacking paired data, we employ the Naturalness Image Quality Evaluator (NIQE) [35].

V. RESULTS

A. LLVIP and BCI Results

We evaluate the performance on the LLVIP dataset in two different ways. The image is either randomly cropped into 512x512, or the full image is resized to 256x256 pixels. We present the results in Table I. Our model outperforms other methods. We also show the qualitative results in Fig. 2. It can be observed that different objects are well represented with slight deterioration in spatial details.

TABLE I
RESULTS ON LLVIP. TEST IMAGE RESOLUTION IS 512×512. (*) REPRESENTS EVALUATION WHERE THE FULL IMAGE WAS RESIZED TO 256×256. HIGHER VALUES INDICATE BETTER PERFORMANCE. BEST METHOD IS HIGHLIGHTED IN BOLD FONT.

Methods	PSNR (dB)	SSIM
CycleGAN [8]	11.22	0.214
BCI [8]	12.19	0.270
pix2pixGAN* [7]	10.76	0.175
Ours	13.11	0.59
Ours*	12.59	0.49

The results for BCI are reported in Table II. Our method performs significantly better in SSIM scores and gives competitive values for PSNR despite being trained on 256x256 and evaluated on 1024x1024 full image. The qualitative results are shown in Fig. 3.

¹<https://sites.google.com/site/vonikakis/datasets>



Fig. 2. Comparison of (a) Visible, (b) Ground Truth Infrared, and (c) Generated Infrared images.

TABLE II
RESULTS ON BCI. TEST IMAGE RESOLUTION IS 1024×1024. BEST METHOD IS HIGHLIGHTED IN BOLD FONT.

Methods	PSNR (dB)	SSIM
CycleGAN [8]	16.20	0.37
\mathcal{L}_{ASP} [19]	17.86	0.50
PSPStain [21]	18.62	0.45
PPT [20]	19.09	0.49
pix2pixHD [8]	19.63	0.47
BCI [8]	21.16	0.47
Ours	18.29	0.63

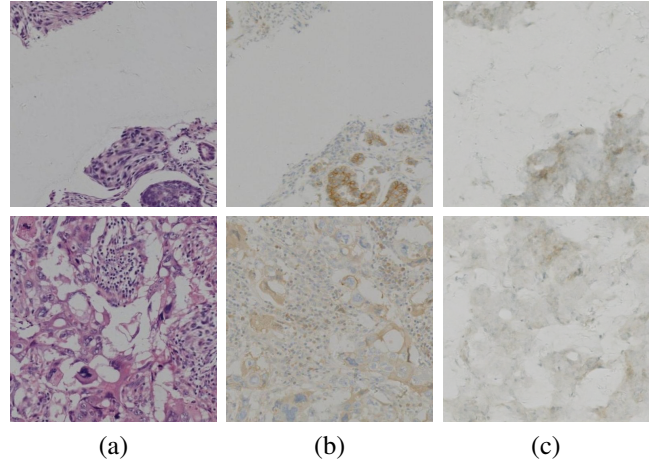


Fig. 3. Comparison of (a) HE, (b) Ground Truth IHC, and (c) Generated IHC images

B. LOL-v1, LOL-v2 and SID Results

We report comparisons for LOLv1, LOLv2-real, and LOLv2-synthetic datasets in Table III. Our method shows a strong performance. However, the results are lower than the SOTA methods. We show the qualitative results in Figure 4. We can see that the generated images closely matches to the ground truth.

The results for the Sony subset of the SID dataset [9] are

TABLE III
COMPARISON WITH SOTA METHODS. BEST METHOD IS HIGHLIGHTED IN BOLD FONT.

Methods	LOL-v1		LOL-v2-real		LOL-v2-synthetic		SID	
	PSNR (dB)	SSIM	PSNR (dB)	SSIM	PSNR (dB)	SSIM	PSNR (dB)	SSIM
SID [9]	14.35	0.43	13.24	0.44	15.04	0.61	16.97	0.59
IPT [36]	16.27	0.50	19.80	0.81	18.30	0.81	20.53	0.56
UFormer [37]	16.36	0.77	18.82	0.77	19.66	0.87	18.54	0.57
Sparse [30]	17.20	0.64	20.06	0.81	22.05	0.90	18.68	0.60
RUAS [38]	18.23	0.72	18.37	0.72	16.55	0.65	18.44	0.58
FIDE [39]	18.27	0.66	16.85	0.67	23.22	0.92	19.02	0.57
AnlightenDiff [26]	21.72	0.81	20.65	0.83	-	-	-	-
Diff-Retinex [24]	21.98	0.86	-	-	-	-	-	-
SNR-Net [40]	24.61	0.84	21.48	0.84	24.14	0.92	22.87	0.62
Retinexformer [41]	25.16	0.84	22.80	0.84	25.67	0.93	24.44	0.68
PyDiff [27]	27.09	0.93	24.01	0.87	19.60	0.87	-	-
GSAD [10]	27.84	0.87	28.82	0.89	28.67	0.94	-	-
Ours	21.10	0.78	22.72	0.79	22.00	0.87	20.97	0.57

shown in Table III. We can see that the proposed method achieves notable performance.

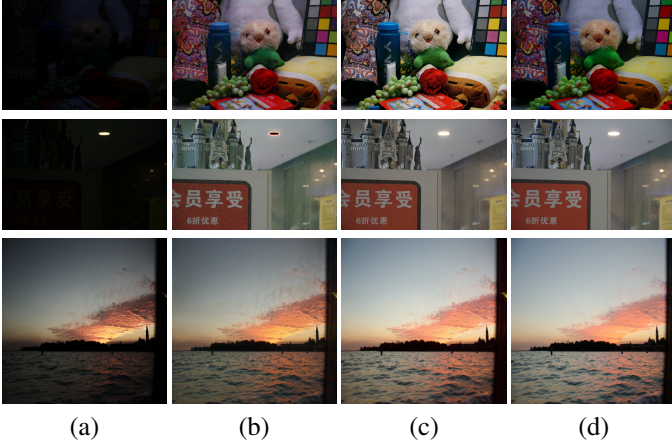


Fig. 4. Comparison of results on different datasets: First row: LoL-v1, Second Row: LoLv2-real, Last row: LoLv2-synthetic. Columns represent: (a) Low-Light Input, (b) RetinexFormer, (c) Ours, and (d) Ground Truth.

TABLE IV
NIQE SCORES ARE COMPUTED WITH THE FULL RESOLUTION OF THE IMAGES. LOWER VALUES INDICATE BETTER PERFORMANCE.

Methods	DICM	LIME	MEF	NPE	VV
EnGAN [22]	3.57	3.71	3.23	4.11	-
KinD [42]	-	3.88	3.34	3.92	-
DCC-Net [43]	3.70	4.42	4.59	3.70	3.28
GSAD [10]	3.28	4.32	3.40	3.55	2.60
Retinexformer [41]	2.85	3.70	3.14	3.64	2.55
Ours	3.09	3.67	2.96	3.65	4.7

C. NIQE Scores

We compare the naturalness image quality (NIQE) across DICM, LIME, MEF, NPE, and VV datasets in Table IV. Our model achieves the best results for LIME and MEF, and the second-best results for DICM. As the model does not see these datasets during training, better NIQE scores indicate



Fig. 5. First row: LIME, Second row: NPE, Third row: MEF, Fourth row: DICM, Last row: VV. Columns: (a) Input Image, (b) RetinexFormer, (c) Ours.

stronger generalization to unseen domains. For VV, a high-resolution dataset, using a model trained on LoLv2-synthetic with 128x128 patches causes a performance drop.

Compared to SOTA method GSAD [10] in LOL-v1 and LOL-v2, we perform better in DICM, LIME and MEF. In case of VV, [10] performs better. Compared to SOTA method Retinexformer [41] in SID, our method does better for LIME and MEF, and gives approximately same performance in NPE. The qualitative results in Fig. 5 clearly show enhanced details.

VI. CONCLUSION

In this work, we introduced Conditional Consistency Models (CCMs) for cross-modal image translation and enhancement tasks. The conditional input guides the denoising process and generates output corresponding to the paired conditional input. Unlike existing methods such as GANs and diffusion models, CCMs achieve superior results without requiring iterative sampling or adversarial training. Distinct from other works, our method can be adopted for different tasks of translation or enhancement and shows competitive results in both the tasks. Extensive experiments on benchmark datasets demonstrate the superior performance of our method. In future, we aim to explore further generalization of CCMs to additional conditional tasks and investigate improvements in conditional guidance mechanisms.

REFERENCES

- [1] Ian Goodfellow, Jean Pouget-Abadie, Mehdi Mirza, Bing Xu, David Warde-Farley, Sherjil Ozair, Aaron Courville, and Yoshua Bengio, “Generative adversarial nets,” in *NeurIPS*, 2014, pp. 2672–2680.
- [2] Jonathan Ho, Ajay Jain, and Pieter Abbeel, “Denoising diffusion probabilistic models,” *NeurIPS*, 2020.
- [3] Mehdi Mirza and Simon Osindero, “Conditional generative adversarial nets,” *arXiv preprint arXiv:1411.1784*, 2014.
- [4] Phillip Isola, Jun-Yan Zhu, Tinghui Zhou, and Alexei A Efros, “Image-to-image translation with conditional adversarial networks,” in *CVPR*, 2017, pp. 1125–1134.
- [5] Jun-Yan Zhu, Taesung Park, Phillip Isola, and Alexei A Efros, “Unpaired image-to-image translation using cycle-consistent adversarial networks,” in *ICCV*, 2017, pp. 2223–2232.
- [6] Yang Song, Prafulla Dhariwal, Mark Chen, and Ilya Sutskever, “Consistency models,” *ICML*, 2023.
- [7] Yujie Zhang, Yunchao Tian, Bo Xiao, Qiong Zhao, and Jia Li, “Llvp: A large-scale low-light visible-infrared paired dataset for image translation,” in *CVPR*, 2021, pp. 12345–12354.
- [8] Shengjie Liu, Chuang Zhu, Feng Xu, Xinyu Jia, Zhongyue Shi, and Mulan Jin, “Bci: Breast cancer immunohistochemical image generation through pyramid pix2pix,” in *CVPRW*, 2022, pp. 1815–1824.
- [9] Chen Chen, Qifeng Chen, and Vladlen Koltun, “Learning to see in the dark,” in *CVPR*, 2018.
- [10] Jinhui Hou, Zhiyu Zhu, Junhui Hou, Hui Liu, Huanqiang Zeng, and Hui Yuan, “Global structure-aware diffusion process for low-light image enhancement,” *NeurIPS*, vol. 36, 2024.
- [11] Edwin H Land and John J McCann, “Lightness and retinex theory,” *Josa*, vol. 61, no. 1, 1971.
- [12] Chitwan Saharia, Jonathan Ho, William Chan, Tim Salimans, David J Fleet, and Mohammad Norouzi, “Image super-resolution via iterative refinement,” *TPAMI*, vol. 45, no. 4, pp. 4713–4726, 2022.
- [13] Tong Che, Yanran Li, Athul Paul Jacob, Yoshua Bengio, and Wenjie Li, “Mode regularized generative adversarial networks,” *ICLR*, 2017.
- [14] Vladimir V Kniaz, Vladimir A Knyaz, Jiri Hladuvka, Walter G Kropatsch, and Vladimir Mizginov, “Thermalgan: Multimodal color-to-thermal image translation for person re-identification in multispectral dataset,” in *ECCVW*, 2018.
- [15] Decao Ma, Shaopeng Li, Juan Su, Yong Xian, and Tao Zhang, “Visible-to-infrared image translation for matching tasks,” *IEEE Journal of Selected Topics in Applied Earth Observations and Remote Sensing*, 2024.
- [16] Mehmet Akif Özkanoglu and Sedat Ozer, “Infragan: A gan architecture to transfer visible images to infrared domain,” *Pattern Recognition Letters*, vol. 155, pp. 69–76, 2022.
- [17] Haining Wang, Na Li, Huijie Zhao, Yan Wen, Yi Su, and Yuqiang Fang, “Mappingformer: Learning cross-modal feature mapping for visible-to-infrared image translation,” in *ACM MM*, 2024, pp. 10745–10754.
- [18] Guoqing Zhu, Honghu Pan, Qiang Wang, Chao Tian, Chao Yang, and Zhenyu He, “Data generation scheme for thermal modality with edge-guided adversarial conditional diffusion model,” in *ACM MM*, 2024, pp. 10544–10553.
- [19] Fangda Li, Zhiqiang Hu, Wen Chen, and Avinash Kak, “Adaptive supervised patchnce loss for learning h&e-to-ihc stain translation with inconsistent groundtruth image pairs,” in *MICCAI*, 2023.
- [20] Wei Zhang, Tik Ho Hui, Pui Ying Tse, Fraser Hill, Condon Lau, and Xinyue Li, “High-resolution medical image translation via patch alignment-based bidirectional contrastive learning,” in *MICCAI*, 2024, pp. 178–188.
- [21] Fuqiang Chen, Ranran Zhang, Boyun Zheng, Yiwen Sun, Jiahui He, and Wenjian Qin, “Pathological semantics-preserving learning for h&e-to-ihc virtual staining,” in *MICCAI*, 2024, pp. 384–394.
- [22] Yifan Jiang, Xinyu Gong, Ding Liu, Yu Cheng, Chen Fang, Xiaohui Shen, Jianchao Yang, Pan Zhou, and Zhangyang Wang, “Enlightengan: Deep light enhancement without paired supervision,” *IEEE TIP*, vol. 30, pp. 2340–2349, 2021.
- [23] Shuzhou Yang, Moxuan Ding, Yanmin Wu, Zihan Li, and Jian Zhang, “Implicit neural representation for cooperative low-light image enhancement,” in *ICCV*, 2023, pp. 12918–12927.
- [24] Xunpeng Yi, Han Xu, Hao Zhang, Linfeng Tang, and Jiayi Ma, “Diff-retinex: Rethinking low-light image enhancement with a generative diffusion model,” in *ICCV*, 2023, pp. 12302–12311.
- [25] Yufei Wang, Yi Yu, Wenhan Yang, Lanqing Guo, Lap-Pui Chau, Alex C Kot, and Bihan Wen, “Exposurediffusion: Learning to expose for low-light image enhancement,” in *ICCV*, 2023, pp. 12438–12448.
- [26] Cheuk-Yiu Chan, Wan-Chi Siu, Yuk-Hee Chan, and H Anthony Chan, “Anlightendiff: Anchoring diffusion probabilistic model on low light image enhancement,” *TIP*, 2024.
- [27] Dewei Zhou, Zongxin Yang, and Yi Yang, “Pyramid diffusion models for low-light image enhancement,” *IJCAI*, 2023.
- [28] Yang Song and Prafulla Dhariwal, “Improved techniques for training consistency models,” *ICLR*, 2023.
- [29] Chen Wei, Wenjing Wang, Wenhan Yang, and Jiaying Liu, “Deep retinex decomposition for low-light enhancement,” in *BMVC*, 2018.
- [30] Wenhan Yang, Wenjing Wang, Haofeng Huang, Shiqi Wang, and Jiaying Liu, “Sparse gradient regularized deep retinex network for robust low-light image enhancement,” *TIP*, 2021.
- [31] Xinhao Guo, Yu Li, and Haibin Ling, “Lime: Low-light image enhancement via illumination map estimation,” *IEEE TIP*, vol. 26, no. 2, pp. 982–993, 2016.
- [32] Shuhang Wang, Jin Zheng, Hai-Miao Hu, and Bo Li, “Naturalness preserved enhancement algorithm for non-uniform illumination images,” *IEEE TIP*, vol. 22, no. 9, pp. 3538–3548, 2013.
- [33] Kede Ma, Kai Zeng, and Zhou Wang, “Perceptual quality assessment for multi-exposure image fusion,” *IEEE TIP*, vol. 24, no. 11, pp. 3345–3356, 2015.
- [34] Chulwoo Lee, Chul Lee, and Chang-Su Kim, “Contrast enhancement based on layered difference representation of 2d histograms,” *IEEE TIP*, vol. 22, no. 12, pp. 5372–5384, 2013.
- [35] Anish Mittal, Rajiv Soundararajan, and Alan C. Bovik, “Making a ‘completely blind’ image quality analyzer,” *IEEE Signal Processing Letters*, vol. 20, no. 3, pp. 209–212, 2013.
- [36] Hanting Chen, Yunhe Wang, Tianyu Guo, Chang Xu, Yiping Deng, Zhenhua Liu, Siwei Ma, Chunjing Xu, Chao Xu, and Wen Gao, “Pre-trained image processing transformer,” in *CVPR*, 2021.
- [37] Zhendong Wang, Xiaodong Cun, Jianmin Bao, and Jianzhuang Liu, “Uformer: A general u-shaped transformer for image restoration,” in *CVPR*, 2022.
- [38] Risheng Liu, Long Ma, Jiaao Zhang, Xin Fan, and Zhongxuan Luo, “Retinex-inspired unrolling with cooperative prior architecture search for low-light image enhancement,” in *CVPR*, 2021.
- [39] Ke Xu, Xin Yang, Baocai Yin, and Rynson WH Lau, “Learning to restore low-light images via decomposition-and-enhancement,” in *CVPR*, 2020.
- [40] Xiaogang Xu, Ruixing Wang, Chi-Wing Fu, and Jiaya Jia, “Snr-aware low-light image enhancement,” in *CVPR*, 2022, pp. 17693–17703.
- [41] Yuanhao Cai, Hao Bian, Jing Lin, Haoqian Wang, Radu Timofte, and Yulun Zhang, “Retinexformer: One-stage Retinex-based Transformer for Low-light Image Enhancement,” in *ICCV*, 2023, pp. 12470–12479.
- [42] Yonghua Zhang, Jiawan Zhang, and Xiaojie Guo, “Kindling the darkness: A practical low-light image enhancer,” in *ACM MM*, 2019, pp. 1632–1640.
- [43] Zhao Zhang, Huan Zheng, Richang Hong, Mingliang Xu, Shuicheng Yan, and Meng Wang, “Deep color consistent network for low-light image enhancement,” in *CVPR*, 2022.